

UC San Diego

UC San Diego Previously Published Works

Title

Exploration of the 2,3-dihydroisoindole pharmacophore for inhibition of the influenza virus PA endonuclease

Permalink

<https://escholarship.org/uc/item/93g3n2pn>

Authors

Rogolino, Dominga
Naesens, Lieve
Bartoli, Jennifer
et al.

Publication Date

2021-11-01

DOI

10.1016/j.bioorg.2021.105388

Peer reviewed



HHS Public Access

Author manuscript

Bioorg Chem. Author manuscript; available in PMC 2022 November 01.

Published in final edited form as:

Bioorg Chem. 2021 November ; 116: 105388. doi:10.1016/j.bioorg.2021.105388.

Exploration of the 2,3-Dihydroisoindole Pharmacophore for Inhibition of the Influenza Virus PA Endonuclease

Dominga Rogolino^{*,a,#}, Lieve Naesens^{*,b,#}, Jennifer Bartoli^a, Mauro Carcelli^a, Laura De Luca^c, Giorgio Pelosi^a, Ryjul W. Stokes^d, Ria Van Berwaer^b, Serena Vittorio^c, Annelies Stevaert^b, Seth M. Cohen^d

^aDepartment of Chemistry, Life Sciences and Environmental Sustainability, University of Parma, and CIRCMSB (Consorzio Interuniversitario di Ricerca in Chimica dei Metalli nei Sistemi Biologici) Parma Unit, 43124, Parma, Italy

^bRega Institute for Medical Research, KU Leuven – University of Leuven, B-3000, Leuven, Belgium

^cDipartimento di Scienze Chimiche, Biologiche, Farmaceutiche e Ambientali, Polo Universitario SS. Annunziata, Università di Messina, Viale Palatucci 13, Messina, I-98168, Italy

^dDepartment of Chemistry and Biochemistry, University of California, San Diego, La Jolla, California 92093, United States

Abstract

Seasonal influenza A and B viruses represent a global concern. Antiviral drugs are crucial to treat severe influenza in high-risk patients and prevent virus spread in case of a pandemic. The emergence of viruses showing drug resistance, in particular for the recently licensed polymerase inhibitor baloxavir marboxil, drives the need for developing alternative antivirals. The endonuclease activity residing in the N-terminal domain of the polymerase acidic protein (PA_N) is crucial for viral RNA synthesis and a validated target for drug design. Its function can be impaired by molecules bearing a metal-binding pharmacophore (MBP) able to coordinate the two divalent metal ions in the active site. In the present work, the 2,3-dihydro-6,7-dihydroxy-1H-isoindol-1-one scaffold is explored for the inhibition of influenza virus PA endonuclease. The structure-activity relationship was analysed by modifying the substituents on the lipophilic moiety linked to the MBP. The new compounds exhibited nanomolar inhibitory activity in a FRET-based enzymatic assay, and a few compounds (**15-17, 21**) offered inhibition in the micromolar range, in a cell-based influenza virus polymerase assay. When investigated against a panel of PA-mutant forms, compound **17** was shown to retain full activity against the baloxavir-resistant I38T mutant.

*Corresponding authors: dominga.rogolino@unipr.it (D. Rogolino); lieve.naesens@kuleuven.be (L. Naesens).

#These authors contributed equally.

Author Contributions

The manuscript was written through contributions of all authors. All authors have given approval to the final version of the manuscript.

Declaration of competing interest

S.M.C. is a cofounder of and has an equity interest in Cleave Therapeutics and Forge Therapeutics, companies that may potentially benefit from the research results. S.M.C. also serves on the Scientific Advisory Board for Forge Therapeutics. The terms of this arrangement have been reviewed and approved by the University of California, San Diego in accordance with its conflict of interest policies.

This was corroborated by docking studies providing insight into the binding mode of this novel class of PA inhibitors.

Keywords

influenza virus; endonuclease; antiviral; isoindolinone; metal-binding pharmacophore

1. Introduction

Seasonal influenza A and B viruses cause 3 to 5 million cases of severe illness and 290,000-650,000 deaths each year [1]. In addition, influenza A viruses are responsible for occasional pandemics, such as the Spanish flu of 1918 or the flu pandemic of 2009 [2,3]. Because influenza vaccines offer only partial protection [4], antiviral drugs are crucial to treat severe influenza in high-risk patients, and prevent virus spread in the case of a pandemic. For many years, this was limited to two drug classes: Matrix-2 (M2) proton channel inhibitors and neuraminidase inhibitors (NAIs). The first class became superfluous after global spread of resistant viruses [5]. NAIs such as oseltamivir are the standard of care in most countries [6], but due to their suboptimal efficacy [7] and potential susceptibility to resistance [8] the development of alternative agents is warranted. The polymerase inhibitors favipiravir and baloxavir (full name: baloxavir marboxil, BXM) were recently licensed in a few countries [9,10,11]. In Figure 1 it is reported the chemical structure of Baloxavir acid (BXA), the active form of the oral prodrug BXM, obtained by development of a lead dihydrodibenzothiepine pharmacophore [12]. It is a particularly potent inhibitor of influenza A and B viruses, showing nanomolar activity in cell culture and higher efficacy than oseltamivir in patients [13,14]. Still, baloxavir-resistant mutants are now commonly detected during therapy [15,16,17]. Although some of these mutations appear to impact viral fitness, the high transmissibility of baloxavir-resistant influenza viruses is quite concerning [18,19].

The ~200 residues long N-terminal domain of the viral PA protein (PA_N) is endowed with endonuclease activity [20,21]. Together with PB1 and PB2, PA forms the influenza virus polymerase, the enzyme complex responsible for transcription and replication of the negative-sense viral RNA genome [22,23,24]. Viral transcription proceeds via a 'cap-snatching' mechanism, in which PB2 binds a capped host cell RNA, which is cleaved by the PA endonuclease to generate a 5'-capped primer for synthesis of viral mRNA by the PB1 polymerase [25,26]. The discovery that PA_N has a unique fold [20,21] and depends on two divalent metal ions (Mn²⁺ or Mg²⁺) [27] to perform its endonuclease activity inspired the development of inhibitors that combine a metal-binding pharmacophore (MBP) with hydrophobic substituents, to occupy the pockets surrounding the PA_N catalytic core [28,29,30]. Co-crystallographic analysis of BXA in complex with the PA_N protein of influenza A or B virus demonstrates its tight-fitting binding mode [31,32,33] and, furthermore, rationalizes the fast selection of resistant viruses bearing mutations I38T/M/F/N/R [15,16]. To address the need for alternative PA inhibitors that are not cross-resistant with BXA, other scaffolds can be explored by exploiting variations

in the MBP in terms of disposition and nature of donor atoms, and in the structure of the hydrophobic moiety that is needed for tight binding to PA_N.

A wide range of structurally diverse PA_N inhibitors have been reported in the literature [23]. Some of the most relevant prototypes are depicted in Figure 1, with the MBP highlighted in red. Most reported inhibitors carry a tridentate MBP, like baloxavir, diketoacid derivatives [34,35] (e.g. L-742,001), flutimide [36], *N*-hydroxyimides [37], 4,5-Dihydroxypyrimidine-6-Carboxamides [38], salicyl amide derivatives [39] or polyhydroxylated *N*-acylhydrazones [40]. A few known PA_N inhibitors possess a bidentate MBP (e.g., 5-hydroxypyrimidin-4-ones [41,42] and 5-hydroxypyridin-4-ones [43]).

Despite structural heterogeneity, all these inhibitors share a common design, consisting of an MBP to coordinate the metal ions within the PA_N catalytic site, and a hydrophobic moiety to interact with the surrounding pockets and ensure efficient binding of the inhibitor. The strategy of impairing enzyme function through metal cofactor binding has been proved to be successful for the development of inhibitors of other viral metalloenzymes that require divalent cations to perform their function [44,45]. Hence, based on the functional homology between the active sites of PA_N endonuclease, HIV integrase, HIV RNase H, and HCV NS5B polymerase, inhibitors developed against one of these targets may possibly be optimized towards another viral target via structure-based scaffold repurposing [46,47]. This strategy has the advantage of using structures with established synthetic procedures that could be tailored to improve selectivity towards the desired target [48].

In the present work, attention was focused on the 2,3-dihydro-6,7-dihydroxy-1H-isindol-1-one scaffold, previously disclosed for inhibition of HIV integrase [49]. The repurposing of these compounds towards PA_N was inspired by favorable features in their skeleton, such as the three oxygen donor atoms with high affinity for Mg²⁺/Mn²⁺ and a suitable preorganization (i.e., well-defined geometry and rigidity) to chelate both metal ions. Additionally, it was reasoned that the lipophilic benzyl portion could be decorated with appropriate substituents to engage in favorable interactions with amino acid residues of PA_N and increase inhibitory activity (Figure 2). Finally, to the best of our knowledge, this scaffold has not yet been investigated for inhibition of influenza virus or PA_N endonuclease.

Herein, a series of 2,3-dihydroisindole derivatives (**14-23**, Scheme 1) bearing different substituents on the aromatic portion of the core structure were synthesized. Both hydrogen bond donors and acceptors, as well as π -stacking naphthalene groups were investigated to develop preliminary structure-activity relationship (Scheme 1). Several analogues exhibited nanomolar activity in a FRET-based PA_N enzymatic assay, and a few offered selective inhibition in a cell-based influenza virus polymerase assay. Interestingly, these compounds retained full activity against the BXA-resistant I38T PA-mutant. Docking studies were also performed to gain insight into the PA_N binding mode of this class of metal-chelating inhibitors.

2. Results and discussion

2.1 Chemistry

The synthesis of the isoindol-1-ones **14-23** was accomplished according to literature procedures, with some modifications (Scheme 1) [49].

The ¹H-NMR spectrum of intermediates **1** and **2** are reported in Figure S1. Intermediate **3** was combined with the desired benzylamine in acetonitrile in the presence of triethylamine, to afford the 6,7-dimethoxy derivatives **4-13**.

Crystals suitable for X-ray analysis were obtained for intermediate **5** and the crystal structure is reported in Figure S2.

The final compounds **14-23** (Scheme 1) were obtained by adding BBr₃ dropwise to a solution of the 6,7-dimethoxy intermediate in CH₂Cl₂ under an inert atmosphere. Deprotection was verified by ¹H NMR; for example, where the two singlets associated with the methoxy groups at 4.15 and 3.91 ppm of **4** (dark arrows, Figure S3) disappeared in the spectrum of the deprotected compound 6,7-dihydroxy **14**. A corresponding broad signal at 5.55 ppm appeared in **14**, which can be attributed to the two hydroxyl groups (red arrow, Figure S3). Furthermore, crystals of **14** suitable for X-ray diffraction analysis were obtained by slow evaporation of a methanolic solution (Figure 3 and Figure S4), which confirmed the overall composition of the compound.

2.2 Inhibitory activity against PA_N enzyme

To assess inhibition of PA_N endonuclease activity, a fluorescence quenching-based assay was used [43]. As shown in Table 1, all compounds in the series showed strong inhibition of PA_N, exhibiting nanomolar activity. The variations introduced in the aromatic moiety had some, though relatively small, impact on activity. Namely, a half maximal inhibitory concentration (IC₅₀) value in the range of 23-46 nM was obtained for the unsubstituted benzyl analogue **14**, as well as the analogues bearing 5-Cl (**15**), 4-Me (**16**), 4-OH (**17**), 4-F (**18**), and 4-NO₂ (**20**) substituents. The 4-CF₃ substitution (**19**) was disadvantageous, reducing activity by a factor 9 when compared to the 4-F analogue **18**. When the benzyl group is replaced by a bulkier naphthyl moiety, the position of this group seems important. The 2-naphthyl analogue **21** showed an IC₅₀ value of 30 nM, which is in the same range as the benzyl analogues. By contrast, activity was reduced 4-fold for the 1-naphthyl analogue **22**. Finally, inhibitory activity was not altered by adding one extra carbon atom to the spacer between the isoindolinone moiety and aromatic ring, since comparable IC₅₀ values were noted for **23** and **17**.

2.3 Inhibition of influenza virus polymerase activity in the minigenome assay

To assess inhibition of PA endonuclease activity in cells, the viral ribonucleoprotein (vRNP) reconstitution ('minigenome') assay was used. The compounds were added to HEK293T cells transfected with four plasmids encoding the PB1, PB2 and PA polymerase components and the nucleoprotein, plus a luciferase reporter plasmid [28,35]. In parallel, compound cytotoxicity was estimated in mock-transfected cells. We included three reference

compounds: BXA, the diketo acid-based PA_N inhibitor L-742,001, [50] and RNA synthesis inhibitor ribavirin. Similar to what was observed in the PA_N enzyme assay, all the isoindol-1-one derivatives proved to be active. An EC₅₀ value of ~4 μM was recorded for four compounds in the series, namely the substituted benzyl analogues **15**, **16**, and **17**, and 2-naphthyl analogue **21** (Table 2). Activity was 3- to 7-fold lower for the other analogues. The favourable selectivity was evident from the finding that, except for **23**, all the analogues showed a CC₅₀ value >100 μM (highest concentration tested). Compounds **15-17** and **21** were equipotent to the prototype PA inhibitor L-742,001 (EC₅₀: 5 μM); however, they had >2,000-fold lower cell culture activity than BXA. The activity shift between the enzyme versus cellular assay was indeed quite pronounced (for example, for **15**, the EC₅₀/IC₅₀ ratio was 145). This is commonly observed for experimental PA_N inhibitors [23] and is plausibly explained by low cell permeability.

2.4 Evaluation against mutant forms of PA, including the BXA-resistant I38T mutant

As done previously with L-742,001 [28], we applied the minigenome assay to determine the inhibitory effect towards mutant forms of PA, bearing substitutions in the PA_N catalytic core or surrounding hydrophobic pockets. Compound **17** and the three reference compounds were selected for these resistance experiments. Table 3 shows the fold increase in EC₅₀ value for mutant versus wild-type PA, and Figure 4 shows the corresponding dose-response curves. As expected, the I38T mutant exhibited pronounced, 65-fold, resistance to BXA. In contrast, for compound **17**, L-742,001, and ribavirin, the EC₅₀ values were comparable for PA-I38T mutant and wild-type polymerase. The activity of **17** was reduced (i.e., EC₅₀ increased by a factor 4 to 6) by mutations in the PA_N catalytic core, namely H41A, G81T, R84L, I120T, V122T, R124Q and K137L. This corroborates that **17** owes its activity in the minigenome assay to inhibition of PA. On the other hand, **17** was not affected by the T20A mutation, which confers weak (i.e., 3-fold) resistance to L-742,001. Vice versa, the R84L mutation rendered 4-fold resistance to **17**, but had no impact on the EC₅₀ value of L-742,001. As expected, the activity of ribavirin was not affected by any of the PA mutations.

2.5 Docking studies

To investigate the binding mode of the 2,3-dihydroisoindole derivatives, docking studies were performed on compound **17** by means of Gold software [51], employing the 3D coordinates of the crystal structure of PA_N in complex with epigallocatechin 3-gallate (EGCG) (PDB code 4AWM) [52]. To perform docking with **17**, we used a procedure (see Experimental Section for all details) that was previously validated by redocking L-742,001, for which we adequately reproduced the binding mode established by crystallography [40, 54]. The docking results show that **17** plausibly binds to PA_N with its benzyl group located in a pocket lined by Arg84 (Figure 5, Panel A), with which it appears to form van der Waals interactions. This can explain why substituting this Arg into Leu (i.e., mutant R84L) led to a 3.8-fold increase in EC₅₀ value for **17**. Notably, in our model, the positively charged side chain of Arg84 is quite close to the carboxylate moiety of Glu23, which may stabilize the orientation of Arg84 and favour van der Waals interactions between this residue and compound **17**. We hypothesize that removing the interaction with Glu23, by introducing a Leu at position 84, should result in a weaker interaction with the ligand.

In our docking model (Figure 5, Panel B), **17** chelates the two metal ions through its two hydroxyl groups and its carbonyl group in a similar way as seen for the diketo acid compound L-742,001 (PDB code 4E5H) [30]. The 2,3-dihydroisoindole system can engage in aromatic interactions with His41, providing an explanation for the 4.9-fold resistance to **17**, when His41 is substituted by Ala. Furthermore, **17** forms two hydrogen bonds between i) the hydroxyl group of its benzyl portion and the backbone of Leu106 and ii) the 6-hydroxyl group of its isoindole moiety and the side chain of Lys134. Finally, van der Waals interactions were observed with Trp88, Phe105, Ile120 and Gly121. Differently from L-742,001, mutation T20A did not impair the inhibitory activity of **17**, which is consistent with our docking model in which the region around Ala20 was not involved in binding **17**.

3. Conclusion

Due to emerging antiviral drug resistance, new influenza virus inhibitors are urgently needed. The PA_N endonuclease is a validated drug target and diverse classes of chemical compounds targeting its catalytic function have already been reported. These scaffolds combine a metal-binding pharmacophore to coordinate the two metal ions in the active site, with a lipophilic moiety to ensure tight binding in the surrounding pockets. Based on the functional homology between the active sites of PA_N endonuclease and HIV integrase, the 2,3-dihydro-6,7-dihydroxy-1H-isoindol-1-one scaffold, previously disclosed for inhibition of HIV integrase [49] was explored. Compounds **14-23** were shown to exhibit nanomolar activity in a fluorescence-quenching enzymatic assay, and among this series, **15-17** and **21** proved to have a favourable profile in the minigenome assay, with EC₅₀ values of ~4 μM and no cytotoxicity at 100 μM. This lower cell culture activity is plausibly explained by relatively poor cell permeability, as is not unusual with PA_N inhibitors [23]. Importantly, resistance experiments established that compound **17** has a different resistance profile than BXA and L-742,001, and especially its unaltered activity against the BXA-resistant I38T mutant is remarkable. The biological resistance data are supported by docking analysis, which indicated that the benzyl group of compound **17** binds to a pocket lined by Arg84, while its two hydroxyls and carbonyl group are engaged in metal ion chelation. This validates our docking model as a relevant basis for further lead optimization.

Hence, besides confirming the strength of inhibitor repurposing, our study establishes the 2,3-dihydro-6,7-dihydroxy-1H-isoindol-1-one scaffold as a versatile metal-binding pharmacophore. This structure appears highly relevant to develop alternative influenza virus PA inhibitors and address the resistance issue of existing agents like baloxavir.

4. Experimental

4.1 Chemistry

All reagents of commercial quality were purchased from Sigma-Aldrich and used without further purification. The purity of the synthesized compounds was determined by elemental analysis and verified to be 95%, by using a FlashSmart CHNS analyzer (Thermo Fisher) with gas-chromatographic separation. ¹H-NMR spectra were recorded at 25 °C on a Bruker Advance 500 or 400 MHz FT spectrometer. The ATR-IR spectra were recorded by means of a Spectrum Two (Perkin Elmer) spectrophotometer by using a diamond crystal plate in

the range of 4000–400 cm^{-1} . Mass spectrometry experiments were performed by using an Agilent 6230 Accurate-Mass LC-TOF MS at the U.C. San Diego Molecular Mass Spectrometry Facility.

1,2-dimethoxy-4-(methoxymethyl)benzene, (1): In a Schleck flask, under N_2 atmosphere, 3,4-dimethoxy-benzyl alcohol (3.74 mL, 1 eq, 25.7 mmol) is dissolved in dry THF and it is cooled to 0°C . Sodium hydride 99% (1.0 g, 1 eq, 25.7 mmol) is added portion-wise to the solution which turns to grey. It is left reacting for 30 minutes at 0°C . Iodomethane (2.09 mL, 1.3 eq, 33.4 mol) is added dropwise to the solution, which is allowed to return to room temperature and it is left reacting for 3 hours, monitoring by TLC (Hex:AcOEt, 8:2). The reaction is quenched by ice-water and ethyl acetate addition. The organic phase is washed with water, then brine, and it is dried on MgSO_4 . After salt removal, solution is taken to dryness by vacuum and the residue dark brown oil is purified by column chromatography (Hex:AcOEt, 8:2) to give the product as a colorless oil (yield = 96%). $^1\text{H-NMR}$ (CDCl_3 -d, 500 MHz, 25°C), ppm: 6.87–6.79 (m, 3H, CH_{arom}), 4.36 (s, 2H, CH_2), 3.86 (s, 3H, OCH_3), 3.84 (s, 3H, OCH_3), 3.34 (s, 3H, OCH_3). $^{13}\text{C-NMR}$ (CDCl_3 -d, 125 MHz, 25°C), ppm: 149.10, 148.68, 130.84, 120.40, 111.05, 110.92, 74.70, 57.98, 56.01, 55.85.

Methyl-2,3-dimethoxy-6-(methoxymethyl)benzoate, (2): In a Schleck flask, under N_2 atmosphere, (1) (2.001 g, 1 eq, 10.98 mmol) is dissolved in dry diethyl ether (30 mL); the mixture is cooled to 0°C ; n-butyl lithium (1.6 M solution in hexane) (10 mL, 1.5 eq, 16.48 mmol) is added dropwise to the solution, which becomes cream-colored. It is left reacting for 3 hours. The solution is cooled to -78°C and methyl chloroformate (4.00 mL, 4.7 eq, 51.61 mmol) is added; it is allowed to return to r.t., and it is left reacting for 20 hours. Water is added until the solution becomes colorless; the organic phase is extracted, dried with MgSO_4 , filtered and the solvent is removed by vacuum. The residual oil is purified by column chromatography (Hex:AcOEt, 1:1), to give the product as a pale yellow oil (yield = 42%). $^1\text{H-NMR}$ (CDCl_3 -d, 500 MHz, 25°C), ppm: 7.04 (d, $J = 5$ Hz, 1H, CH_{arom}), 6.90 (d, $J = 5$ Hz, 1H, CH_{arom}), 4.39 (s, 2H, CH_2), 3.91 (s, 3H, OCH_3), 3.86 (s, 6H, OCH_3), 3.32 (s, 3H, OCH_3). $^{13}\text{C-NMR}$ (CDCl_3 -d, 125 MHz, 25°C), ppm: 186.78, 167.92, 152.43, 128.43, 128.13, 124.35, 113.29, 72.22, 61.65, 58.29, 56.04, 52.30.

Methyl 6-(chloromethyl)-2,3-dimethoxybenzoate, (3): In a round bottom flask, (2) (1.0329 g, 1 eq, 4.2991 mmol) is dissolved in dry diethyl ether (5 mL), together with dry zinc(II) chloride (352 mg, 0.601 eq, 2.58 mmol); the solution is cooled to 0°C . Then, acetyl chloride (990 μL , 3.24 eq, 13.9 mmol) is added dropwise to the solution, which turns to orange; the mixture is left reacting for 30 minutes at 0°C . Aluminum(III) oxide (1.0 g, 2.3 eq, 9.8 mmol) is added and the mixture is filtered on a small pad of Al_2O_3 . The solvent is completely removed, and the residual oil is purified by column chromatography (Hex:AcOEt, 1:1) to give a pale yellow oil (yield = 64%). $^1\text{H-NMR}$ (CDCl_3 -d, 500 MHz, 25°C), ppm: 7.11 (d, $J = 10$ Hz, 1H, CH_{arom}), 6.92 (d, $J = 10$ Hz, 1H, CH_{arom}), 4.59 (s, 2H, CH_2), 3.95 (s, 3H, OCH_3), 3.88 (s, 6H, OCH_3). $^{13}\text{C-NMR}$ (CDCl_3 -d, 125 MHz, 25°C), ppm: 1167.33, 153.19, 146.91, 128.77, 127.52, 125.95, 113.51, 61.68, 56.04, 52.60, 43.78.

General procedure for the synthesis of 6,7-dimethoxyisoindolin-1-ones: **(3)** is dissolved in acetonitrile (6 mL) and triethylamine (2 eq) is added; the mixture is heated up to reflux. An equimolar amount of the proper amine is added, and the mixture is left reacting for 7-10 hours at reflux. The solvent is removed by rotavapor and the residue is portioned between water and CH₂Cl₂; the organic phase is extracted and dried with MgSO₄, filtered on a Buchner funnel and dried by vacuum. The residue is purified by column chromatography (Hex:AcOEt, 1:1).

2-benzyl-6,7-dimethoxyisoindolin-1-one, (4): yellow powder (yield = 52%). ¹H-NMR (CDCl₃-d, 500 MHz, 25°C), ppm: 7.34-7.25 (m, 5H, CH_{arom}), 7.06 (d, J = 10 Hz, 1H, CH_{arom}), 6.99 (d, J = 10 Hz, 1H, CH_{arom}), 4.74 (s, 2H, CH₂), 4.15 (s, 2H, CH₂), 4.11 (s, 3H, CH₃), 3.88 (s, 3H, CH₃). ¹³C-NMR (CDCl₃-d, 125 MHz, 25°C), ppm: 166.77, 152.44, 147.48, 137.20, 134.60, 128.84, 128.33, 127.71, 124.95, 117.85, 116.54, 62.70, 56.89, 48.57, 46.44. ESI-TOF MS: m/z = 306.11 (M+Na⁺). M.p.: 85-87°C.

2-(3-chloro-4-fluorobenzyl)-6,7-dimethoxyisoindolin-1-one, (5): yellow powder (yield = 20%). ¹H-NMR (CDCl₃-d, 500 MHz, 25°C), ppm: 7.35 (d, J = 10 Hz, 1H, CH_{arom}), 7.20-7.17 (m, 1H, CH_{arom}), 7.11-7.07 (m, 2H, CH_{arom}), 7.03 (d, J = 10 Hz, 1H, CH_{arom}), 4.66 (s, 2H, CH₂), 4.16 (s, 2H, CH₂), 4.08 (s, 3H, OCH₃), 3.86 (s, 3H, OCH₃). ¹³C-NMR (CDCl₃-d, 125 MHz, 25°C), ppm: 166.85, 158.67, 152.56, 147.55, 134.37 (d, J = 7.2 Hz), 130.38, 128.07 (d, J = 6.3 Hz), 124.62, 121.21 (d, J = 15.0 Hz), 117.96, 117.05, 116.88, 116.79, 62.65, 56.89, 48.59, 45.41. ESI-TOF MS: m/z = 358.06 (M+Na⁺). Crystals suitable for X-ray analysis were obtained for intermediate **5** from slow evaporation of a solution of the compound (Hex:AcOEt, 3:7).

2-(4-methylbenzyl)-6,7-dimethoxyisoindolin-1-one, (6): yellow powder (yield= 40%). ¹H-NMR (CDCl₃-d, 500 MHz, 25°C), ppm: 7.20 (d, J = 10 Hz, 2H, CH_{arom}), 7.13 (d, J = 10 Hz, 2H, CH_{arom}), 7.05 (d, J = 10 Hz, 1H, CH_{arom}), 6.98 (d, J = 5 Hz, 1H, CH_{arom}), 4.70 (s, 2H, CH₂), 4.14 (s, 2H, CH₂), 4.11 (s, 3H, OCH₃), 3.87 (s, 3H, OCH₃), 2.32 (s, 3H, CH₃). ¹³C-NMR (CDCl₃-d, 125 MHz, 25°C), ppm: 166.70, 152.39, 147.39, 137.38, 134.67, 134.17, 129.47, 128.33, 125.01, 117.86, 116.47, 62.65, 56.85, 48.49, 46.12, 21.18. ESI-TOF MS: m/z = 320.12 (M+Na⁺).

2-(4-hydroxybenzyl)-6,7-dimethoxyisoindolin-1-one, (7): yellow powder (yield= 51%). ¹H-NMR (CDCl₃-d, 500 MHz, 25°C), ppm: 7.14 (d, J = 5 Hz, 2H, CH_{arom}), 7.06 (d, J = 10 Hz, 1H, CH_{arom}), 7.00 (d, J = 10 Hz, 1H, CH_{arom}), 6.80 (d, J = 5 Hz, 2H, CH_{arom}), 4.65 (s, 2H, CH₂), 4.15 (s, 2H, CH₂), 4.08 (s, 3H, OCH₃), 3.87 (s, 3H, OCH₃). ¹³C-NMR (CDCl₃-d, 125 MHz, 25°C), ppm: 167.03, 156.10, 152.44, 147.31, 134.59, 129.64, 128.38, 124.92, 122.50, 117.95, 116.68, 115.87, 62.56, 56.85, 48.67, 46.10. ESI-TOF MS: m/z = 322.10 (M+Na⁺).

2-(4-fluorobenzyl)-6,7-dimethoxyisoindolin-1-one, (8): pale-orange powder (yield= 32%). ¹H-NMR (CDCl₃-d, 500 MHz, 25°C), ppm: 7.29-7.27 (m, 2H, CH_{arom}), 7.06 (d, J = 5 Hz, 1H, CH_{arom}), 7.02-6.98 (m, 3H, CH_{arom}), 4.70 (s, 2H, CH₂), 4.15 (s, 2H, CH₂), 4.10 (s, 3H, OCH₃), 3.88 (s, 3H, OCH₃). ¹³C-NMR (CDCl₃-d, 125 MHz, 25°C), ppm: 166.77, 163.31, 161.35, 152.45, 147.39, 134.48, 133.05 (d, J = 3.0 Hz), 129.99 (d, J = 8.8 Hz),

124.81, 117.97, 116.59, 115.75, 115.58, 62.61, 56.82, 48.51, 45.66. ESI-TOF MS: $m/z=324.10$ ($M+Na^+$).

2-(4-(trifluoromethyl)benzyl)-6,7-dimethoxy-isoindolin-1-one, (9): pale-yellow powder (yield = 47%). 1H -NMR ($CDCl_3$ -d, 400 MHz, 25°C), ppm: 7.57 (d, $J = 4$ Hz, 2H, CH_{arom}), 7.41 (d, $J = 4$ Hz, 2H, CH_{arom}), 7.08 (d, 1H, $J = 8$ Hz, CH_{arom}), 7.01 (d, $J = 8$ Hz, 1H, CH_{arom}), 4.79 (s, 2H, CH_2), 4.17 (s, 2H, CH_2), 4.10 (s, 3H, OCH₃), 3.88 (s, 3H, OCH₃). ^{13}C -NMR ($CDCl_3$ -d, 100 MHz, 25°C), ppm: 166.94, 152.58, 147.64, 141.34, 134.40, 129.95, 128.49, 125.83 (d, $J = 3.0$ Hz), 124.60, 117.89, 116.87, 62.63, 55.97, 56.91, 48.67, 46.05. Anal. Calcd. for $C_{18}H_{16}F_3NO_3 \cdot H_2O$: C 58.54, H 4.91, N 3.79. Found: C 58.41, H 5.12, N 3.65.

2-(4-nitrobenzyl)-6,7-dimethoxy-isoindolin-1-one, (10): white powder (yield=10%). 1H -NMR ($CDCl_3$ -d, 400 MHz, 25°C), ppm: 8.17 (d, $J = 8$ Hz, 2H, CH_{arom}), 7.46 (d, $J = 8$ Hz, 2H, CH_{arom}), 7.09 (d, $J = 4$ Hz, 1H, CH_{arom}), 7.03 (d, $J = 4$ Hz, 1H, CH_{arom}), 4.83 (s, 2H, CH_2), 4.20 (s, 2H, CH_2), 4.09 (s, 3H, OCH₃), 3.88 (s, 3H, OCH₃). ^{13}C -NMR ($CDCl_3$ -d, 100 MHz, 25°C), ppm: 166.87, 152.43, 147.44, 141.36, 134.20, 129.93, 128.49, 125.81, 124.60, 117.55, 115.76, 62.63, 56.91, 48.67, 46.05. Anal. Calcd. for $C_{17}H_{16}N_2O_5 \cdot \frac{3}{4} H_2O$: C 59.73, H 5.16, N 8.20. Found: C 59.46, H 5.16, N 7.55.

2-(naphthalen-2-ylmethyl)-6,7-dimethoxy-isoindolin-1-one, (11): pale-orange powder (yield= 20%). 1H -NMR ($CDCl_3$ -d, 500 MHz, 25°C), ppm: 7.82-7.79 (m, 3H, CH_{arom}), 7.74 (s, 1H, CH_{arom}), 7.48-7.42 (m, 3H, CH_{arom}), 7.05 (d, $J = 5$ Hz, 1H, CH_{arom}), 6.98 (d, $J = 10$ Hz, 1H, CH_{arom}), 4.90 (s, 2H, CH_2), 4.17 (s, 2H, CH_2), 4.14 (s, 3H, OCH₃), 3.88 (s, 3H, OCH₃). ^{13}C -NMR ($CDCl_3$ -d, 126 MHz, 25°C), ppm: 166.88, 152.47, 147.50, 134.74, 134.62, 133.43, 132.94, 128.80, 127.82, 127.07, 126.42, 126.34, 126.12, 124.96, 117.90, 116.59, 62.72, 56.90, 48.63, 46.64. ESI-TOF MS: $m/z=356.12$ ($M+Na^+$).

2-(naphthalen-1-ylmethyl)-6,7-dimethoxy-isoindolin-1-one, (12): yellow powder (yield= 47%). 1H -NMR ($CDCl_3$ -d, 400 MHz, 25°C), ppm: 8.27 (d, 1H, CH_{arom}), 7.87 (t, 2H, CH_{arom}), 7.58-7.44 (m, 4H, CH_{arom}), 7.04 (d, 1H, CH_{arom}), 6.93 (d, 1H, CH_{arom}), 5.22 (s, 2H, CH_2), 4.16 (s, 3H, OCH₃), 4.04 (s, 2H, CH_2), 3.80 (s, 3H, OCH₃). ^{13}C -NMR ($CDCl_3$ -d, 100 MHz, 25°C), ppm: 166.38, 153.18, 142.04, 134.02, 132.16, 132.05, 131.52, 129.22, 128.85, 127.51, 127.04, 126.29, 125.30, 123.62, 119.59, 114.45, 62.74, 56.88, 48.65, 46.64. Anal. Calcd. for $C_{19}H_{15}NO_3 \cdot \frac{4}{3} H_2O$: C 62.13, H 5.76, N 4.53. Found: C 62.56, H 5.57, N 4.36.

2-(4-hydroxyphenethyl)-6,7-dimethoxyisoindolin-1-one, (13): yellow powder (yield=22%). 1H -NMR ($CDCl_3$ -d, 400 MHz, 25°C), ppm: 7.06-6.99 (m, 4H, CH_{arom}), 6.78 (d, $J = 8$ Hz, 2H, CH_{arom}), 6.29 (s, br, OH), 4.13 (s, 2H, CH_2), 4.05 (s, 3H, OCH₃), 3.87 (s, 3H, OCH₃), 3.76 (t, 2H, CH_2), 2.87 (t, 2H, CH_2). ^{13}C -NMR ($CDCl_3$ -d, 100 MHz, 25°C), ppm: 167.05, 154.97, 152.43, 147.35, 134.64, 130.27, 129.78, 125.13, 117.75, 116.62, 115.71, 62.59, 56.90, 49.72, 44.42, 33.90. Anal. Calcd. for $C_{18}H_{19}NO_4 \cdot \frac{1}{2} H_2O$: C 67.07, H 6.25, N 4.35. Found: C 67.23, H 6.15, N 4.23.

General procedure for the synthesis of 6,7-dihydroxyisoindolin-1-ones: 6,7-

dimethoxyisoindolin-1-ones are dissolved in dry dichloromethane (5 mL) in a dried round bottom double-necked flask; the solution is purged with nitrogen flux for 30 min, then it is cooled to -78°C . Boron tribromide 99% (8.5 eq) is slowly added to the solution, which is allowed to return to r.t. After 4 hours, volatiles are eliminated by vacuum, then the solid is quenched with methanol; it is dried by rotovap and the solid is portioned between water and EtO_2 . The organic phase is extracted, washed with water and dried by rotovap to give the final product.

2-benzyl-6,7-dihydroxyisoindolin-1-one, (14): pale-grey powder (yield= 40%). $^1\text{H-NMR}$ ($\text{CDCl}_3\text{-d}$, 500 MHz, 25°C), ppm: 8.36 (s, br, 1H, OH), 7.35-7.25 (m, 5H, CH_{arom}), 7.04 (d, 1H, CH_{arom}), 6.75 (d, 1H, CH_{arom}), 5.51 (s, br, 1H, OH), 4.72 (s, 2H, CH_2), 4.20 (s, 2H, CH_2). $^{13}\text{C-NMR}$ ($\text{CDCl}_3\text{-d}$, 125 MHz, 25°C), ppm: 143.21, 142.07, 136.61, 132.10, 128.97, 128.16, 127.94, 119.67, 117.53, 114.49, 49.80, 46.16. ESI-TOF MS: m/z = 356.09 ($\text{M}+\text{Na}^+$). IR (ATR, cm^{-1}): $\nu(\text{OH})$ = 3336; $\nu(\text{CH}_{\text{arom}})$ = 3028, 2915; $\nu(\text{C}=\text{O})$ = 1661; $\nu(\text{C-N})$ = 1270. Anal. Calcd. for $\text{C}_{15}\text{H}_{13}\text{NO}_3$: C 70.55, H 5.10, N 5.49. Found: C 70.10, H 5.26, N 5.10. M.p.: 148-152 $^{\circ}\text{C}$.

2-(3-chloro-4-fluorobenzyl)-6,7-dihydroxyisoindolin-1-one, (15): beige powder (yield = 90%). $^1\text{H-NMR}$ ($\text{CDCl}_3\text{-d}$, 500 MHz, 25°C), ppm: 8.31 (s, br, 1H, OH), 7.33 (d, J = 10 Hz, 1H, CH_{arom}), 7.17-7.08 (m, 3H, CH_{arom}), 7.06(d, J = 10 Hz, 1H, CH_{arom}), 6.78 (d, J = 10 Hz, 1H, CH_{arom}), 5.86 (s, br, 1H, OH), 4.66 (s, 2H, CH_2), 4.20 (s, 2H, CH_2). $^{13}\text{C-NMR}$ ($\text{CDCl}_3\text{-d}$, 125 MHz, 25°C), ppm: 168.51, 157.98, 156.03, 145.01, 143.55, 136.14, 132.85, 130.32, 128.93, 120.07 (d, J = 13.7 Hz), 118.28, 117.56 (d, J = 20 Hz), 114.29, 49.24, 44.57. ESI-TOF MS: m/z = 308.04 ($\text{M}+\text{H}^+$). IR (ATR, cm^{-1}): ν_{OH} = 3302; $\nu(\text{CH}_{\text{arom}})$ = 2922; $\nu(\text{C}=\text{O})$ = 1660; $\nu(\text{C-N})$ = 1246; $\nu(\text{C-F})$ = 783; $\nu(\text{C-Cl})$ = 668. Anal. Calcd. for $\text{C}_{15}\text{H}_{11}\text{NO}_3\text{FCl}$: C 58.55, H 3.60, N 4.60. Found: C 58.21, H 3.96, N 4.20. M.p.: 157-161 $^{\circ}\text{C}$.

2-(4-methylbenzyl)-6,7-dihydroxy-isoindolin-1-one, (16): beige powder (yield = 85%). $^1\text{H-NMR}$ ($\text{CDCl}_3\text{-d}$, 500 MHz, 25°C), ppm: 8.40 (s, br, 1H, OH), 7.17-7.13 (m, 4H, CH_{arom}), 7.03 (d, J = 10 Hz, 1H, CH_{arom}), 6.74 (d, J = 5 Hz, 1H, CH_{arom}), 5.60 (s, vbr, 1H, OH), 4.67 (s, 2H, CH_2), 4.17 (s, 2H, CH_2), 2.32 (s, 3H, CH_3). $^{13}\text{C-NMR}$ ($\text{CDCl}_3\text{-d}$, 125 MHz, 25°C), ppm: 154.97, 143.25, 142.06, 137.70, 135.42, 133.55, 132.13, 129.62, 128.18, 119.66, 114.46, 49.72, 45.89, 21.18. ESI-TOF MS: m/z = 292.09 ($\text{M}+\text{Na}^+$). IR (ATR, cm^{-1}): $\nu(\text{OH})$ = 3229; $\nu(\text{CH}_{\text{arom}})$ = 2920; $\nu(\text{C}=\text{O})$ = 1640; $\nu(\text{C-N})$ = 1303. Anal. Calcd. for $\text{C}_{18}\text{H}_{19}\text{NO}_3$: C 72.64, H 6.39, N 4.71. Found: C 73.10, H 6.71, N 4.41. M.p.: 124-127 $^{\circ}\text{C}$.

2-(4-hydroxybenzyl)-6,7-dihydroxy-isoindolin-1-one, (17): beige powder (yield = 54%). $^1\text{H-NMR}$ ($\text{CDCl}_3\text{-d}$, 500 MHz, 25°C), ppm: 8.33 (s, br, 1H, OH), 7.20 (d, J = 8 Hz, 2H, CH_{arom}), 7.04 (d, J = 8 Hz, 1H, CH_{arom}), 6.84-6.78 (m, 3H, CH_{arom}), 5.32 (s, br, 1H, OH), 4.64 (s, 2H, CH_2). $^{13}\text{C-NMR}$ ($\text{CDCl}_3\text{-d}$, 125 MHz, 25°C), ppm: 168.38, 157.20, 144.84, 143.43, 132.61, 129.65, 128.14, 120.00, 118.53, 115.89, 114.29, 48.93, 45.08. HR-ESI-TOF MS: m/z = 272.09 ($\text{M}+\text{Na}^+$). IR (ATR, cm^{-1}): $\nu(\text{OH})$ = 3454; $\nu(\text{CH}_{\text{arom}})$ =

2973; $\nu(\text{C}=\text{O}) = 1652$; $\nu(\text{C}-\text{N}) = 1265$. Anal. Calcd. for $\text{C}_{15}\text{H}_{13}\text{NO}_4 \cdot 1/3 \text{H}_2\text{O}$: C 64.98, H 4.97, N 5.05. Found: C 65.02, H 5.21, N 4.65. M.p.: 209-211°C.

2-(4-fluorobenzyl)-6,7-dihydroxyisoindolin-1-one, (18): pale-grey powder (yield = 58%). $^1\text{H-NMR}$ (CDCl_3 -d, 300 MHz, 25°C), ppm: 7.30 (dd, $J = 15$ Hz, 2H, CH_{arom}), 7.17 (dd, $J = 15$ Hz, 2H, CH_{arom}), 6.96 (d, $J = 9$ Hz, 1H, CH_{arom}), 6.76 (d, $J = 9$ Hz, 1H, CH_{arom}), 4.63 (s, 2H, CH_2), 4.19 (s, 2H, CH_2). $^{13}\text{C-NMR}$ (CDCl_3 -d, 125 MHz, 25°C), ppm: 169.80, 143.34, 142.14, 132.44, 131.99, 129.92 (d, $J = 7.5$ Hz), 119.88, 117.42, 115.89 (d, $J = 21.2$ Hz), 114.53, 49.73, 45.47. ESI-TOF MS: $m/z = 274.08$ ($\text{M}+\text{H}^+$). IR (ATR, cm^{-1}): $\nu(\text{OH}) = 3336$; $\nu(\text{CH}_{\text{arom}}) = 2959, 2923, 2857$; $\nu(\text{C}=\text{O}) = 1661$; $\nu(\text{C}-\text{N}) = 1270$; $\nu(\text{C}-\text{F}) = 781$. Anal. Calcd. for $\text{C}_{15}\text{H}_{12}\text{NO}_3\text{F}$: C 65.93, H 4.40, N 5.13. Found: C 65.98, H 4.64, N 4.86. M.p.: 155-158°C.

2-(4-(trifluoromethyl)benzyl)-6,7-dihydroxy-isoindolin-1-one, (19): brown powder (yield=80%). $^1\text{H-NMR}$ (DMSO-d_6 , 400 MHz, 25°C), ppm: 7.89 (d, $J = 4$ Hz, 2H, CH_{arom}), 7.32 (d, $J = 4$ Hz, 2H, CH_{arom}), 6.92 (d, $J = 8$ Hz, 1H, CH_{arom}), 6.74 (d, $J = 8$ Hz, 1H, CH_{arom}), 4.68 (s, 2H, CH_2), 4.21 (s, 2H, CH_2). ESI-TOF-MS (pos ions): $m/z = 324$ [$\text{M}+\text{H}^+$]. Anal. Calcd. for $\text{C}_{16}\text{H}_{12}\text{F}_3\text{NO}_3 \cdot \text{H}_2\text{O}$: C 56.31, H 4.13, N 4.10. Found: C 56.38, H 4.34, N 4.03. M.p.: 109-112°C.

2-(4-nitrobenzyl)-6,7-dihydroxy-isoindolin-1-one, (20): white powder (yield = 24%). $^1\text{H-NMR}$ (CDCl_3 -d, 400 MHz, 25°C), ppm: 8.20 (d, $J = 4$ Hz, 2H, CH_{arom}), 7.45 (d, $J = 4$ Hz, 2H, CH_{arom}), 7.07 (d, $J = 8$ Hz, 1H, CH_{arom}), 6.80 (d, $J = 8$ Hz, 1H, CH_{arom}), 4.82 (s, 2H, CH_2), 4.24 (s, 2H, CH_2). $^{13}\text{C-NMR}$ (CDCl_3 -d, 75 MHz, 25°C), ppm: 170.04, 144.07, 143.45, 142.16, 131.79, 128.73, 124.26, 120.09, 116.98, 114.70, 50.01, 45.60. ESI-TOF-MS (pos ions): $m/z = 323$ [$\text{M}+\text{Na}^+$]. Anal. Calcd. for $\text{C}_{15}\text{H}_{12}\text{N}_2\text{O}_5 \cdot \text{H}_2\text{O}$: C 56.60, H 4.43, N 8.33. Found: C 56.68, H 4.92, N 8.03. M.p.: 160-165°C.

2-(naphthalen-2-ylmethyl)-6,7-dihydroxy-isoindolin-1-one, (21): beige powder (yield = 87%). $^1\text{H-NMR}$ (CDCl_3 -d, 500 MHz, 25°C), ppm: 7.83-7.80 (m, 3H, CH_{arom}), 7.73 (s, 1H, CH_{arom}), 7.49-7.47 (m, 2H, CH_{arom}), 7.40 (d, $J = 8$ Hz, 1H, CH_{arom}), 7.04 (d, $J = 4$ Hz, 1H, CH_{arom}), 6.74 (d, $J = 4$ Hz, 1H, CH_{arom}), 4.88 (s, 2H, CH_2), 4.21 (s, 3H, CH_2). $^{13}\text{C-NMR}$ (CDCl_3 -d, 125 MHz, 25°C), ppm: 166.86, 152.46, 147.48, 134.72, 134.61, 132.41, 132.92, 128.78, 127.81, 127.06, 126.35, 126.09, 124.94, 117.89, 116.58, 62.71, 56.88. ESI-TOF MS: $m/z = 306.11$ ($\text{M}+\text{Na}^+$). IR (ATR, cm^{-1}): $\nu(\text{OH}) = 3166, 3383$; $\nu(\text{CH}_{\text{arom}}) = 2921, 2851$; $\nu(\text{C}=\text{O}) = 1652$; $\nu(\text{C}-\text{N}) = 1259$. Anal. Calcd. for $\text{C}_{19}\text{H}_{15}\text{NO}_3 \cdot 1/8 \text{H}_2\text{O}$: C 74.19, H 5.00, N 4.55. Found: C 74.35, H 5.35, N 4.56. M.p.: 193-196°C.

2-(naphthalen-1-ylmethyl)-6,7-dihydroxy-isoindolin-1-one, (22): pale-beige powder (yield=27%). $^1\text{H-NMR}$ (CDCl_3 -d, 400 MHz, 25°C), ppm: 8.18 (d, $J = 8$ Hz, 1H, CH_{arom}), 7.87-7.83 (m, 2H, CH_{arom}), 7.54 (t, $J = 8$ Hz, 1H, CH_{arom}), 7.50 (t, $J = 8$ Hz, 1H, CH_{arom}), 7.44 (m, 1H, CH_{arom}), 6.99 (d, $J = 4$ Hz, 1H, CH_{arom}), 6.68 (d, $J = 4$ Hz, 1H, CH_{arom}), 5.16 (s, 2H, CH_2), 4.07 (s, 2H, CH_2). $^{13}\text{C-NMR}$ (CDCl_3 -d, 75 MHz, 25°C), ppm: 169.38, 143.18, 142.04, 134.02, 132.17, 132.05, 131.52, 129.22, 128.85, 127.51, 127.04, 126.29, 125.30, 123.62, 119.60, 117.54, 114.45, 49.86, 44.41. ESI-TOF-MS (pos ions): $m/z = 327$ [$\text{M}+\text{Na}^+$]. IR (ATR, cm^{-1}): $\nu(\text{OH}) = 3322$; $\nu(\text{CH}_{\text{arom}}) = 2980, 2920, 2850$; $\nu(\text{C}=\text{O}) =$

= 1652; $\nu(\text{C-N}) = 1259$. Anal. Calcd. for $\text{C}_{19}\text{H}_{15}\text{NO}_3 \cdot 4/3 \text{H}_2\text{O}$: C 62.13, H 5.76, N 4.53. Found: C 62.56, H 5.57, N 4.36. M.p.: 165-167°C.

2-(4-hydroxyphenethyl)-6,7-dihydroxy-isoindolin-1-one, (23): white powder (yield =25%). $^1\text{H-NMR}$ (DMSO-d_6 , 600 MHz, 25°C), ppm: 9.24 (s, 1H, OH), 9.15 (s, 1H, OH), 8.72 (s, 1H, OH), 7.03 (d, $J = 8$ Hz, 2H, CH_{arom}), 6.88 (d, $J = 4$ Hz, 2H, CH_{arom}), 6.72 (d, $J = 4$ Hz, 1H, CH_{arom}), 6.62 (d, $J = 8$ Hz, 1H, CH_{arom}), 4.15 (s, 2H, CH_2), 3.59 (t, $J = 9$ Hz, 2H, $\text{CH}_2\text{-ethyl}$), 2.74 (t, $J = 9$ Hz, 2H, $\text{CH}_2\text{-ethyl}$). $^{13}\text{C-NMR}$ (DMSO-d_6 , 150 MHz, 25°C), ppm: 169.79, 155.77, 144.06, 142.94, 132.65, 129.54, 129.42, 129.39, 119.63, 115.05, 113.54, 50.20, 43.88, 33.42. ESI-TOF-MS (pos ions): $m/z = 308$ $[\text{M}+\text{Na}]^+$. IR (ATR, cm^{-1}): $\nu(\text{OH}) = 3322, 3550, 3480$; $\nu(\text{CH}_{\text{arom}}) = 2917, 2848$; $\nu(\text{C=O}) = 1645$; $\nu(\text{C-N}) = 1224$. Anal. Calcd. for $\text{C}_{19}\text{H}_{15}\text{NO}_3 \cdot 11/4 \text{H}_2\text{O}$: C 64.31, H 5.82, N 3.95. Found: C 64.41, H 5.53, N 3.50. M.p.: 204-209°C.

4.2 Protein Expression and Purification

Pandemic H1N1 N-terminal PA endonuclease was expressed from a pET-28a parent vector containing a kanamycin-resistance reporter gene, expression inducible by the Lac 1 operon. The endonuclease was expressed as an 8-histidine tagged fusion protein. Transformation protocol was adapted from pET system manual (Novagen) using single competent BL21 cells. Briefly, 1 μL of 25 ng/ μL recombinant plasmid was used for transformation. Cells were mixed by flicking with plasmid and were heat shocked at 42 °C for 30 sec followed by incubation on ice for 5 minutes. Outgrowth was plated on LB agarose plates contain 50 $\mu\text{g}/\text{mL}$ kanamycin, and was incubated overnight at 37 °C. One colony was scraped from the LB plate and added to 50 mL of SOC broth containing 50 $\mu\text{g}/\text{mL}$ kanamycin, and was incubated for 5 h at 37 °C with shaking at 125 rpm. Glycerol stocks of this culture were prepared (0.9 mL cultured media + 0.1 mL 80% glycerol) and flash frozen for future expressions. 100 mL of SOC media containing 50 $\mu\text{g}/\text{mL}$ kanamycin was combined with 1 mL frozen glycerol stock or 1 mL the previously mentioned 5 h growth, and was incubated with shaking at 100-125 rpm overnight at 37 °C as a starter culture. This starter culture was then equally divided into 4 \times 1L batches of expression media (TB media with added 0.2% dextrose, 0.1 mM MnCl_2 , and 0.1 mM MgSO_4) containing 50 $\mu\text{g}/\text{mL}$ kanamycin. Cells were grown to the beginning of log phase ($\text{OD}_{600} =$ between 0.6-0.8) at 37 °C with shaking at 100-125 rpm. Expression of PA endonuclease was then induced by the addition of IPTG to a final concentration of 0.8 mM. The media was grown with shaking overnight at ~18 °C. After approximately 18 h the cells were harvested by centrifuging at 2000g for 30 min at 4 °C. The resulting paste was stored at -80 °C prior to lysis.

Cell paste was thawed on ice for 2 h and re-suspended in 25-35 mL of lysis buffer (20 mM Na_2PO_4 , 500 mM NaCl, 25 mM imidazole, 1 mM MgCl_2 , 2 mM dithiothreitol (DTT), 0.2% Triton-X, pH=7.4) plus EDTA free protease inhibitor (Roche) and lysed by sonication - 5 \times 25 sec pulses with 2 min rest periods on ice. To the cell lysates was added DNase1 to a final concentration of 10-100 $\mu\text{g}/\text{mL}$, and the lysates were shaken at 125 rpm for 30-60 min on ice until the consistency of the lysate became free-flowing. Cell debris was then pelleted by centrifugation at 10000 rpm 35-45 min at 4 °C. The supernatant was decanted from the pellet, and a HisTrap HP (Parnacia) column was utilized to isolate His-tagged fusion protein

from the cell lysates according to the manufacturer's recommendations. Briefly, cell-free lysates from 4L of growth were loaded on 1×5mL column that had previously been charged with Ni ions. The column was then washed with binding buffer (20 mM Na₂PO₄, 500 mM NaCl, 25 mM imidazole, pH=7.4) until fraction absorbance reached a steady baseline. Fusion protein was then eluted over a 45 min gradient at a flow rate of 4 mL/min, from 0-100% elution buffer (20 mM Na₂PO₄, 500 mM NaCl, 500 mM imidazole, pH=7.4). Pure target protein eluted between 50-60% elution buffer. Isolated protein was flash-frozen and stored at -80 °C. SDS-PAGE analysis showed a single band of pure protein running at ~23kD.

4.3 Endonuclease Activity Assays

Endonuclease activity assays were carried out in Black Costar 96-well plates. Each well contained a total volume of 100 µL comprised of: buffer (20 mM Tris, 150 mM NaCl, 2 mM MnCl₂, 10 mM β-mercaptoethanol, 0.2% Triton-X100, pH=8.0), influenza PA endonuclease (25 nM), inhibitor (various concentrations) in buffer, and fluorescent ssDNA-oligo substrate (200 nM). A single-stranded, 17-mer DNA substrate labeled with a 5'-FAM fluorophore and a 3'-TAMRA quencher ([6-FAM]AATCGCAGGCAGCACTC[TAM]) synthesized by Sigma-Aldrich was employed as the substrate. All assay components were pipetted into the plate, and ultimately, the substrate was added using a multi-channel pipette, and the assay was immediately started. Background wells consisting of all assay components except enzyme were prepared for each sample. Positive and negative controls were prepared on each plate to gauge the fluorescence signal of fully active protein and the absence of protein. Change in fluorescence of each well was measured by a Synergy H4 Hybrid Multi-Mode Microplate Reader (BioTek) at 39 second intervals over 45 min at 37 °C ($\lambda_{ex} = 485 \text{ nm}$; $\lambda_{em} = 528 \text{ nm}$). The positive control wells contained no inhibitor and were set as an arbitrary 100% activity. The gain was set to 100 and the slope of the fluorescence signal for each sample was background corrected, and percent inhibition was determined by normalizing the slope of the sample to that of the positive and negative controls. Dose response data were analysed using a four-parameter logistic model in the mathematics program MATLAB. The uncertainty of the determined IC₅₀ values is reported as the 95% confidence interval from the linear regression.

4.5 Minigenome assay with mutant forms of PA

To reconstitute vRNP complexes of influenza virus A/PR/8/34, we used the pVP-PA, pVP-PB1, pVP-PB2 and pVP-NP reverse genetics plasmids, generously donated by M. Kim (Korea Research Institute of Chemical Technology), who also provided the pHH21-FLuc reporter plasmid [27]. The QuikChange II site-directed mutagenesis kit (Stratagene) was used to introduce mutations in the pVP-PA plasmid. To perform the minigenome assay, the five plasmids were reverse transfected into HEK293T cells (from Thermo Fisher Scientific), using JetPEI transfection reagent (Polyplus-transfection). The transfected cells (37,500/well) were transferred to white half-area 96-well plates containing 1:2.5 serial dilutions of the test compounds. In parallel, the test compounds were added to a separate plate containing mock-transfected cells. The reference compounds were: ribavirin (Virazole; from ICN Pharmaceuticals.); BXA (from MedChem Express) and L-742,001 (from Life Chemicals). After 24 h incubation at 37°C, luciferase activity was determined using the ONE-Glo

Luciferase Assay (Promega) and Tecan Spark 10M reader, while compound cytotoxicity was assessed on the mock-transfected plate, using the ATPlite 1step Luminescence Assay (PerkinElmer). The 50% effective concentration (EC₅₀) and 50% cytotoxic concentration (CC₅₀) were calculated by nonlinear least-squares regression analysis of the results from three independent experiments using GraphPad Prism software. Statistical significance of differences between the dose-response curves of different mutants versus wild-type, was determined with an extra-sum-of-squares F test (GraphPad Prism). P-values * 0.05; ** 0.01; *** 0.001; **** 0.0001.

4.6 Molecular docking

Docking studies were performed by means of Gold Suite 5.7.1 [51], using the crystal structure of PA_N (derived from pandemic H1N1 influenza virus) in complex with (-)-epigallocatechin gallate (EGCG; PDB code 4AWM) [30]. The ligand and water molecules were removed, and hydrogens were added by Discovery Studio 2.5. Ligand structures were constructed by VEGAZZ suite and optimized by following a conjugate gradient minimization by AMMP calculation, implemented in the VEGAZZ program [53]. Docking simulation was performed by following the same protocol as reported earlier [40,54]. Briefly, the binding site was defined to contain the residues within 15 Å from the original position of EGCG in the crystallographic structure. The side chain of Tyr24 was set as flexible and GoldScore was selected as fitness function. For each ligand, 100 genetic algorithm runs were performed. Solutions differing less than 0.75 Å in terms of RMSD were clustered together. The pose representative of the most populated cluster was chosen for further analysis and representation. The putative ligand-protein interactions were detected through Discovery Studio Visualiser V20 (Dassault Systèmes BIOVIA) [55].

Supplementary Material

Refer to Web version on PubMed Central for supplementary material.

Acknowledgments

D.R. and M.C. thank “Centro Interfacoltà Misure Giuseppe Casnati” of the University of Parma for facilities. The authors acknowledge Dr. Yongxuan Su (U.C. San Diego, Department of Chemistry & Biochemistry, Molecular Mass Spectrometry Facility) for aid with mass spectrometry analysis and Dr. Benjamin L. Dick and Milan Gembicky (U.C. San Diego, Department of Chemistry & Biochemistry, X-ray crystallography facility) for assistance with X-ray data collection and structure determination.

Funding Sources

R. W. S. was supported, in part, by the Graduate Research Fellowship Program (GRFP) from the National Science Foundation (DGE-1650112) and the National Institutes of Health (R01 AI149444). D.R. was supported, in part, by Progetti di ricerca di Rilevante Interesse Nazionale (PRIN, grant N. 2017BMK8JR).

This work has benefited from the equipment and framework of the COMP-HUB Initiative, funded by the ‘Departments of Excellence’ program of the Italian Ministry for Education, University and Research (MIUR, 2018-2022).

REFERENCES

- [1]. Iuliano AD, Roguski KM, Chang HH, Muscatello DJ, Palekar R, Tempia S, Cohen C, Gran JM, Schanzer D, Cowling BJ, Wu P, Kyncl J, Ang LW, Park M, Redlberger-Fritz M, Yu

- H, Espenhain L, Krishnan A, Emukule G, van Asten L, Pereira da Silva S, Aungkulanon S, Buchholz U, Widdowson MA, Bresee JS, Estimates of global seasonal influenza-associated respiratory mortality: a modelling study, *Lancet* (2018), 391 (10127), 1285–1300. 10.1016/s0140-6736(17)33293-2 [PubMed: 29248255]
- [2]. Taubenberger JK, Kash JC, Morens DM, The 1918 influenza pandemic: 100 years of questions answered and unanswered, *Science translational medicine* (2019) 11 (502), eaau5485. 10.1126/scitranslmed.aau5485 [PubMed: 31341062]
- [3]. Neumann G, Noda T, Kawaoka Y, Emergence and pandemic potential of swine-origin H1N1 influenza virus, *Nature* (2009) 459, 931–939. 10.1038/nature08157 [PubMed: 19525932]
- [4]. Treanor JJ, Clinical practice. Influenza vaccination. *N. Engl. J. Med* (2016) 375 (13), 1261–1268. 10.1056/NEJMcp1512870 [PubMed: 27682035]
- [5]. Moscona A, Medical management of influenza infection, *Annu. Rev. Med* (2008) 59, 397–413. 10.1146/annurev.med.59.061506.213121 [PubMed: 17939760]
- [6]. Nguyen-Van-Tam JS, Venkatesan S, Muthuri SG, Myles PR, Neuraminidase inhibitors: who, when, where?, *Clin. Microbiol. Infect* (2015) 21 (3), 222–225. 10.1016/j.cmi.2014.11.020 [PubMed: 25703253]
- [7]. Muthuri SG, Venkatesan S, Myles PR, Leonardi-Bee J, Al Khuwaitir TSA, Al Mamun A, Ano vadiya AP, Azziz-Baumgartner E, Báez C, Bassetti M, Beovic B, Bertisch B, Bonmarin I, Booy R, Borja-Aburto VH, Burgmann H, Cao B, Carratala J, Denholm JT, Dominguez SR, Duarte PAD, Dubnov-Raz G, Echavarría M, Fanella S, Gao Z, Gérardin P, Giannella M, Gubbels S, Herberg J, Iglesias ALH, Hoger PH, Hu X, Islam QT, Jiménez MF, Kandeel A, Keijzers G, Khalili H, Knight M, Kudo K, Kuszniertz G, Kuzman I, Kwan AMC, Amine IL, Langenegger E, Lankarani KB, Leo Y-S, Linko R, Liu P, Madanat F, Mayo-Montero E, McGeer A, Memish Z, Metan G, Mickiene A, Miki D, Mohn KGI, Moradi A, Nymadawa P, Oliva ME, Ozkan M, Parekh D, Paul M, Polack FP, Rath BA, Rodríguez AH, Sarrouf EB, Seale AC, Sertogullarindan B, Siqueira MM, Skrzypczyk Magierło J, Stephan F, Talarek E, Tang JW, To KKW, Torres A, Törün SH, Tran D, Uyeki TM, Van Zwol A, Vaudry W, Vidmar T, Yokota RTC, Zarogoulidis P, Nguyen-Van-Tam JS, Effectiveness of neuraminidase inhibitors in reducing mortality in patients admitted to hospital with influenza A H1N1pdm09 virus infection: a meta-analysis of individual participant data, *The Lancet Respiratory Medicine* (2014) 2 (5), 395–404. 10.1016/S2213-2600(14)70041-4. [PubMed: 24815805]
- [8]. Lee N, Hurt AC, Neuraminidase inhibitor resistance in influenza: a clinical perspective, *Curr. Opin. Infect. Dis* (2018) 31(6), 520–526. 10.1097/QCO.0000000000000498. [PubMed: 30299356]
- [9]. Furuta Y, Gowen BB, Takahashi K, Shiraki K, Smee DF, Barnard DL, Favipiravir (T-705), a novel viral RNA polymerase inhibitor, *Antiviral Res.* (2013) 100 (2), 446–54. 10.1016/j.antiviral.2013.09.015 [PubMed: 24084488]
- [10]. Shirley M, Baloxavir marboxil: a review in acute uncomplicated influenza, *Drugs* (2020) 80 (11), 1109–1118. 10.1007/s40265-020-01350-8 [PubMed: 32601915]
- [11]. Mifsud EJ, Hayden FG, Hurt AC, Antivirals targeting the polymerase complex of influenza viruses, *Antiviral Res.* (2019) 169, 104545. 10.1016/j.antiviral.2019.104545 [PubMed: 31247246]
- [12]. Taoda Y, Miyagawa M, Akiyama T, Tomita K, Hasegawa Y, Yoshida R, Noshi T, Shishido T, Kawai M, Dihydrodibenzothiepine: Promising hydrophobic pharmacophore in the influenza cap-dependent endonuclease inhibitor, *Bioorg. Med. Chem. Lett* (2020) 15;30(22),127547. doi: 10.1016/j.bmcl.2020.127547.
- [13]. Hayden FG, Sugaya N, Hirotsu N, Lee N, de Jong MD, Hurt AC, Ishida T, Sekino H, Yamada K, Portsmouth S, Kawaguchi K, Shishido T, Arai M, Tsuchiya K, Uehara T, Watanabe A, Baloxavir marboxil for uncomplicated influenza in adults and adolescents, *N. Engl. J. Med* (2018) 379 (10), 913–923. 10.1056/NEJMoal716197 [PubMed: 30184455]
- [14]. Hayden FG, Shindo N, Influenza virus polymerase inhibitors in clinical development, *Curr. Opin. Infect. Dis* (2019) 32 (2), 176–186. 10.1097/QCO.0000000000000532 [PubMed: 30724789]
- [15]. Omoto S, Speranzini V, Hashimoto T, Noshi T, Yamaguchi H, Kawai M, Kawaguchi K, Uehara T, Shishido T, Naito A, Cusack S, Characterization of influenza virus variants induced by

- treatment with the endonuclease inhibitor baloxavir marboxil, *Sci. Rep* (2018) 8, 9633. 10.1038/s41598-018-27890-4 [PubMed: 29941893]
- [16]. Ince WL, Smith FB, O'Rear JJ, Thomson M, Treatment-Emergent Influenza Virus Polymerase Acidic Substitutions Independent of Those at I38 Associated With Reduced Baloxavir Susceptibility and Virus Rebound in Trials of Baloxavir Marboxil, *J. Inf. Dis* (2020) 222, 957–961, 10.1093/infdis/jiaa164 [PubMed: 32253432]
- [17]. Hashimoto T, Baba K, Inoue K, Okane M, Hata S, Shishido T, Naito A, Wildum S, Omoto S, Comprehensive assessment of amino acid substitutions in the trimeric RNA polymerase complex of influenza A virus detected in clinical trials of baloxavir marboxil. *Influenza Other Respir. Viruses* (2020) 15, 1–7. 10.1111/irv.12821
- [18]. Jones JC, Pascua PNQ, Fabrizio TP, Marathe BM, Seiler P, Barman S, Webby RJ, Webster RG, Govorkova EA, Influenza A and B viruses with reduced baloxavir susceptibility display attenuated in vitro fitness but retain ferret transmissibility. *Proc. Natl. Acad. Sci U. S. A* (2020) 117 (15), 8593–8601. 10.1073/pnas.1916825117 [PubMed: 32217734]
- [19]. Imai M, Yamashita M, Sakai-Tagawa Y, Iwatsuki-Horimoto K, Kiso M, Murakami J, Yasuhara A, Takada K, Ito M, Nakajima N, Takahashi K, Lopes TJS, Dutta J, Khan Z, Kriti D, van Bakel H, Tokita A, Hagiwara H, Izumida N, Kuroki H, Nishino T, Wada N, Koga M, Adachi E, Jubishi D, Hasegawa H, Kawaoka Y, Influenza A variants with reduced susceptibility to baloxavir isolated from Japanese patients are fit and transmit through respiratory droplets. *Nat. Microbiol* (2020) 5, 27–33. 10.1038/s41564-019-0609-0 [PubMed: 31768027]
- [20]. Dias A, Bouvier D, Crépin T, McCarthy AA, Hart DJ, Baudin F, Cusack S, Ruigrok RW, The cap-snatching endonuclease of influenza virus polymerase resides in the PA subunit, *Nature* (2009) 458, 914–8. 10.1038/nature07745 [PubMed: 19194459]
- [21]. Yuan P, Bartlam M, Lou Z, Chen S, Zhou J, He X, Lv Z, Ge R, Li X, Deng T, Fodor E, Rao Z, Liu Y, Crystal structure of an avian influenza polymerase PA(N) reveals an endonuclease active site, *Nature* 2009, 458, 909–913. 10.1038/nature07720 [PubMed: 19194458]
- [22]. Pflug A, Lukarska M, Resa-Infante P, Reich S, Cusack S, Structural insights into RNA synthesis by the influenza virus transcription-replication machine, *Virus Res.* (2017) 234, 103–117. 10.1016/j.virusres.2017.01.013. [PubMed: 28115197]
- [23]. Stevaert A, Naesens L, The influenza virus polymerase complex: an update on its structure, functions, and significance for antiviral drug design, *Med. Res. Rev* (2016) 36(6), 1127–1173. 10.1002/med.21401 [PubMed: 27569399]
- [24]. Te Velthuis AJ, Fodor E, Influenza virus RNA polymerase: insights into the mechanisms of viral RNA synthesis, *Nat. Rev. Microbiol* (2016) 14(8), 479–493. 10.1038/nrmicro.2016.87 [PubMed: 27396566]
- [25]. Wandzik JM, Kouba T, Karuppasamy M, Pflug A, Drncova P, Provaznik J, Azevedo N, Cusack S, A structure-based model for the complete transcription cycle of influenza polymerase, *Cell* (2020) 181(4), 877–893. 10.1016/j.cell.2020.03.061 [PubMed: 32304664]
- [26]. Reich S, Guilligay D, Pflug A, Malet H, Berger I, Crépin T, Hart D, Lunardi T, Nanao M, Ruigrok RW, Cusack S, Structural insight into cap-snatching and RNA synthesis by influenza polymerase, *Nature* (2014) 516, 361–366. 10.1038/nature14009 [PubMed: 25409151]
- [27]. Crépin T, Dias A, Palencia A, Swale C, Cusack S, Ruigrok RW, Mutational and metal binding analysis of the endonuclease domain of the influenza virus polymerase PA subunit, *J. Virol* (2010) 84 (18), 9096–9104. 10.1128/JVI.00995-10 [PubMed: 20592097]
- [28]. Stevaert A, Dallochio R, Dessi A, Pala N, Rogolino D, Sechi M, Naesens L, Mutational Analysis of the Binding Pockets of the Diketo Acid Inhibitor L-742,001 in the Influenza Virus PA Endonuclease, *J. Virol* (2013) 87 (19), 10524–10538. 10.1128/JVI.00832-13 [PubMed: 23824822]
- [29]. Kowalinski E, Zubieta C, Wolkerstorfer A, Szolar OHJ, Ruigrok RWH, Cusack S, Structural analysis of specific metal chelating inhibitor binding to the endonuclease domain of influenza pH1N1 (2009) polymerase, *Plos Pathogens* (2012) 8(8), e1002831. 10.1371/journal.ppat.1002831 [PubMed: 22876177]
- [30]. DuBois RM, Slavish PJ, Baughman BM, Yun MK, Bao J, Webby RJ, Webb TR, White SW, Structural and biochemical basis for development of influenza virus inhibitors targeting the PA

endonuclease, PLoS Pathogens (2012), 8(8), e1002830. 10.1371/journal.ppat.1002830 [PubMed: 22876176]

- [31]. Noshi T, Kitano M, Taniguchi K, Yamamoto A, Omoto S, Baba K, Hashimoto T, Ishida K, Kushima Y, Hattori K, Kawai M, Yoshida R, Kobayashi M, Yoshinaga T, Sato A, Okamatsu M, Sakoda Y, Kida H, Shishido T, Naito A, In vitro characterization of baloxavir acid, a first-in-class cap-dependent endonuclease inhibitor of the influenza virus polymerase PA subunit, Antivir Res. (2018) 160, 109–117. 10.1016/j.antiviral.2018.10.008. [PubMed: 30316915]
- [32]. Todd B, Tchesnokov EP, Götte M, The active form of the influenza cap-snatching endonuclease inhibitor baloxavir marboxil is a tight binding inhibitor, J. Biol. Chem (2021) 296, 100486. 10.1016/j.jbc.2021.100486. [PubMed: 33647314]
- [33]. Kumar G, Cuypers M, Webby RR, Webb TR, White SW, Structural insights into the substrate specificity of the endonuclease activity of the influenza virus cap-snatching mechanism. Nucleic Acids Res. (2021) 49(3), 1609–1618. 10.1093/nar/gkaa1294. [PubMed: 33469660]
- [34]. Hastings JC, Selnick H, Wolanski B, Tomassini JE, Anti-influenza virus activities of 4-substituted 2,4-dioxobutanoic acid inhibitors, Antimicrob. Agents Chemother (1996) 40, 1304–1307. 10.1128/AAC.40.5.1304 [PubMed: 8723491]
- [35]. Stevaert A, Nurra S, Pala N, Carcelli M, Rogolino D, Shepard C, Domaoal RA, Kim B, Alfonso-Prieto M, Marras SA, Sechi M, Naesens L, An integrated biological approach to guide the development of metal-chelating inhibitors of influenza virus PA endonuclease, Mol. Pharmacol (2015) 87, 323–337. 10.1124/mol.114.095588. [PubMed: 25477342]
- [36]. Tomassini JE, Davies ME, Hastings JC, Lingham R, Mojena M, Raghoobar SL, Singh SB, Tkacz JS, Goetz MA, A novel antiviral agent which inhibits the endonuclease of influenza viruses, Antimicrob. Agents Chemother (1996) 40, 1189–1193. 10.1128/AAC.40.5.1189 [PubMed: 8723464]
- [37]. Parkes KE, Ermert P, Fassler J, Ives J, Martin JA, Merrett JH, Obrecht D, Williams G, Klumpp K, Use of a pharmacophore model to discover a new class of influenza endonuclease inhibitors. J. Med. Chem (2003) 46, 1153–1164. 10.1021/jm020334u. [PubMed: 12646026]
- [38]. Beylkin D, Kumar G, Zhou W, Park J, Jeevan T, Lagiseti C, Harfoot R, Webby RJ, White SW, Webb TR, Protein-Structure Assisted Optimization of 4,5-Dihydropyrimidine-6-Carboxamide Inhibitors of Influenza Virus Endonuclease, Scientific Reports (2017) 7, 17139. 10.1038/s41598-017-17419-6 [PubMed: 29215062]
- [39]. Carcelli M, Rogolino D, Bacchi A, Rispoli G, Fiscaro E, Compari C, Sechi M, Stevaert A, Naesens L, Metal-chelating 2-hydroxyphenyl amide pharmacophore for inhibition of influenza virus endonuclease. Mol. Pharmaceutics (2014) 11, 304–316. 10.1021/mp400482a
- [40]. Carcelli M, Rogolino D, Gatti A, De Luca L, Sechi M, Kumar G, White SW, Stevaert A, Naesens L, N-acylhydrazone inhibitors of influenza virus PA endonuclease with versatile metal binding modes. Sci. Rep (2016) 6, 31500. 10.1038/srep31500 [PubMed: 27510745]
- [41]. Parhi AK, Xiang A, Bauman JD, Patel D, Vijayan RS, Das K, Arnold E, J. E, Lavoie Phenyl substituted 3-hydroxypyridin-2(1H)-ones: inhibitors of influenza A endonuclease. Bioorg. Med. Chem (2013) 21, 6435–6446. 10.1016/j.bmc.2013.08.053 [PubMed: 24055080]
- [42]. Sagong HY, Bauman JD, Patel D, Das K, Arnold E, LaVoie EJ, Phenyl substituted 4-hydroxypyridazin-3(2H)-ones and 5-hydroxypyrimidin-4(3H)-ones: inhibitors of influenza A endonuclease. J. Med. Chem (2014) 57, 8086–8098. 10.1021/jm500958x [PubMed: 25225968]
- [43]. Credille CV, Chen Y, Cohen SM, Fragment-based identification of influenza endonuclease inhibitors. J. Med. Chem (2016) 59, 6444–6454. doi: 10.1021/acs.jmedchem.9b00747 [PubMed: 27291165]
- [44]. Rogolino D, Carcelli M, Sechi M, Neamati N, Viral enzymes containing magnesium: Metal binding as a successful strategy in drug design. Coord. Chem. Rev (2012) 256 (23-24), 3063–3086. 10.1016/j.ccr.2012.07.006
- [45]. Chen AY, Adamek RN, Dick BL, Credille CV, Morrison CN, Cohen SM, Targeting metalloenzymes for therapeutic intervention. Chem. Rev (2019) 119(2), 1323–1455. 10.1021/acs.chemrev.8b00201 [PubMed: 30192523]

- [46]. Zhao F, Liu N, Zhan P, Liu X, Repurposing of HDAC inhibitors toward anti-hepatitis C virus drug discovery: teaching an old dog new tricks. *Future Med. Chem* (2015) 7, 1367–1371. doi: 10.4155/fmc.15.76 [PubMed: 26230876]
- [47]. Carcelli M, Rogolino D, Gatti A, Pala N, Corona A, Caredda A, Tramontano E, Pannecouque C, Naesens L, Esposito F, Chelation motifs affecting metal-dependent viral enzymes: - acylhydrazone ligands as dual target inhibitors of HIV-1 integrase and reverse transcriptase ribonuclease H domain, *Front. Microbiol* (2017) 8, 440. doi: 10.3389/fmicb.2017.00440 [PubMed: 28373864]
- [48]. Song Y, Chen W, Kang D, Zhang Q, Zhan P, Liu X, “Old friends in new guise”: exploiting privileged structures for scaffold reevolution/refining. *Comb. Chem. High Throughput Screen.* (2014) 17, 536–553. doi: 10.2174/1386207317666140122101631 [PubMed: 24446784]
- [49]. Zhao XZ, Semenova EA, Vu BC, Maddali K, Marchand C, Hughes SH, Pommier Y, Burke TR, 2,3-Dihydro-6,7-dihydroxy-1H-isoindol-1-one-Based HIV-1 Integrase Inhibitors, *J. Med. Chem* (2008) 51, 251–259. 10.1021/jm070715d [PubMed: 18095643]
- [50]. Tomassini JE, Selnick H, Davies ME, Armstrong ME, Baldwin J, Bourgeois M, Hastings J, Hazuda D, Lewis J, McClements W, Ponticello G, Radzilowski E, Smith G, Tebben A, Wolfe A, Inhibition of cap (m7GpppXm)-dependent endonuclease of influenza virus by 4-substituted 2,4-dioxobutanoic acid compounds, *Antimicrob. Agents Chemothe.r* (1994) 38 (12), 2827–37. doi: 10.1128/aac.38.12.2827
- [51]. Jones G, Willett P, Glen RC, Leach AR, Taylor R, Development and validation of a genetic algorithm for flexible docking, *J. Mol. Biol.* 1997, 267, 727–748, doi: 10.1006/jmbi.1996.0897 [PubMed: 9126849]
- [52]. Kowalinski E, Zubieta C, Wolkerstorfer A, Szolar OHJ, Ruigrok RWH, Cusack S, Structural Analysis of Specific Metal Chelating Inhibitor Binding to the Endonuclease Domain of Influenza pH1N1 (2009) Polymerase, *Plos Pathogens*, 2012, 8(8), e1002831. 10.1371/journal.ppat.1002831 [PubMed: 22876177]
- [53]. Pedretti A, Villa L, Vistoli G, VEGA - An open platform to develop chemo-bio-informatics applications, using plug-in architecture and script programming. *J. Comput. Aid Mol. Des* (2004) 18, 167–173. 10.1023/B:JCAM.0000035186.90683.f2
- [54]. Rogolino D, Bacchi A, De Luca L, Rispoli G, Sechi M, Stevaert A, Naesens L, Carcelli M, Investigation of the salicylaldehyde thiosemicarbazone scaffold for inhibition of influenza virus PA endonuclease. *J. Biol. Inorg. Chem* (2015) 20, 1109–1121. doi: 10.1007/s00775-015-1292-0 [PubMed: 26323352]
- [55]. BIOVIA Discovery Studio Visualizer, v20. San Diego: Dassault Systèmes; 2020.

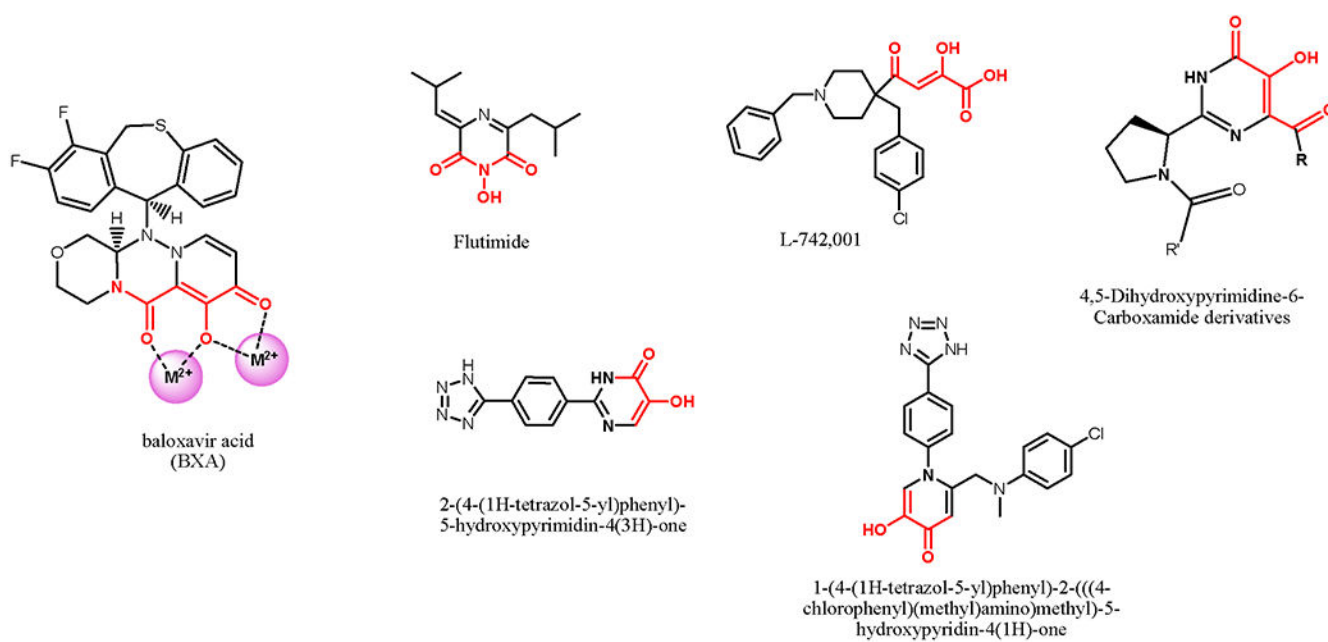


Figure 1. Chemical structures of the approved PA_N inhibitor baloxavir acid and of some prototypic inhibitors. For each compound, the metal-binding group (MBP) is highlighted in red.

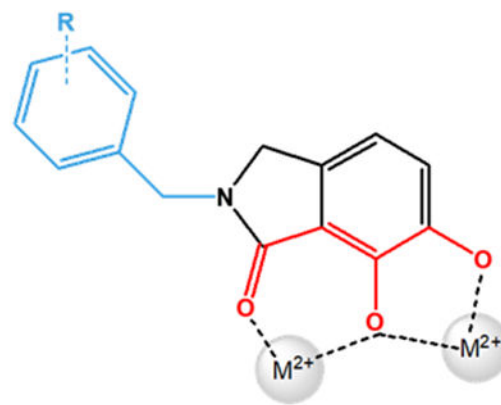
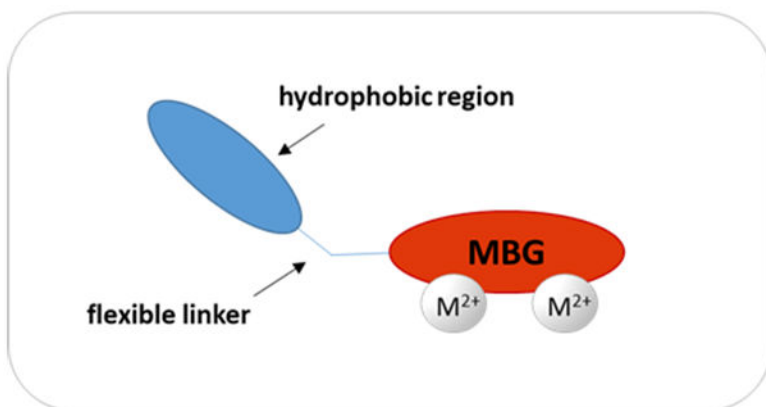


Figure 2.
Chemical scaffold of the 2,3-dihydroisoindole derivatives studied, with metal binding group (MBG) highlighted in red.

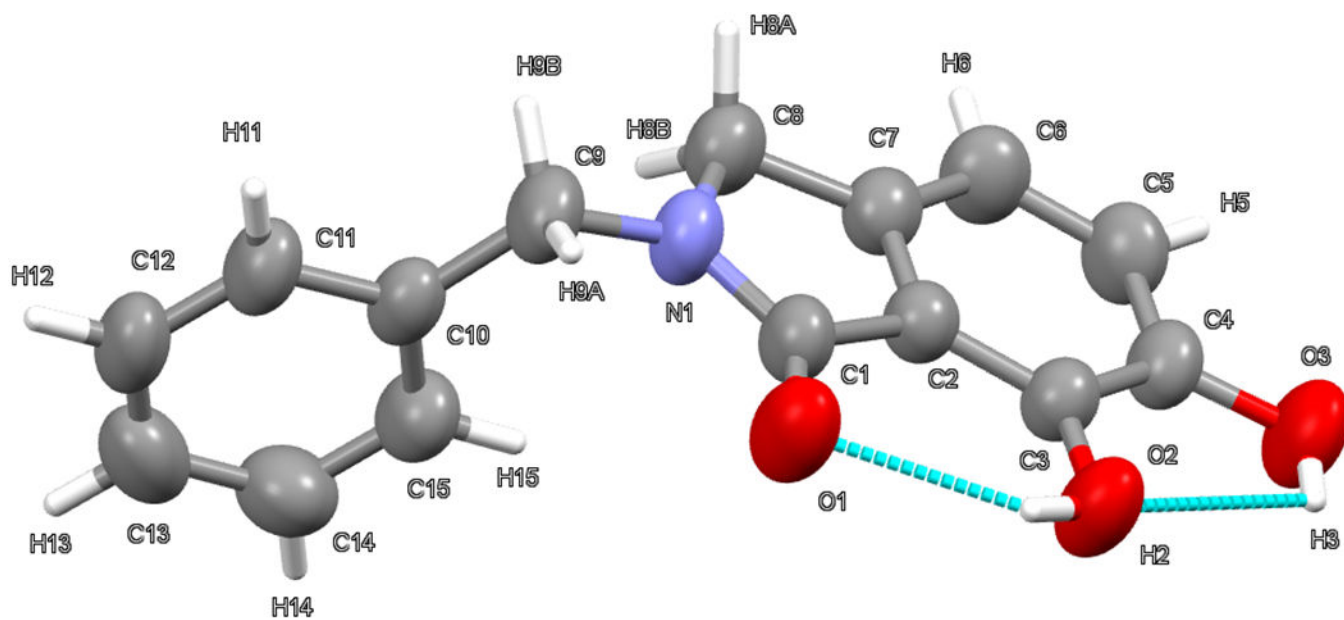


Figure 3.
Crystal structure of **14**.

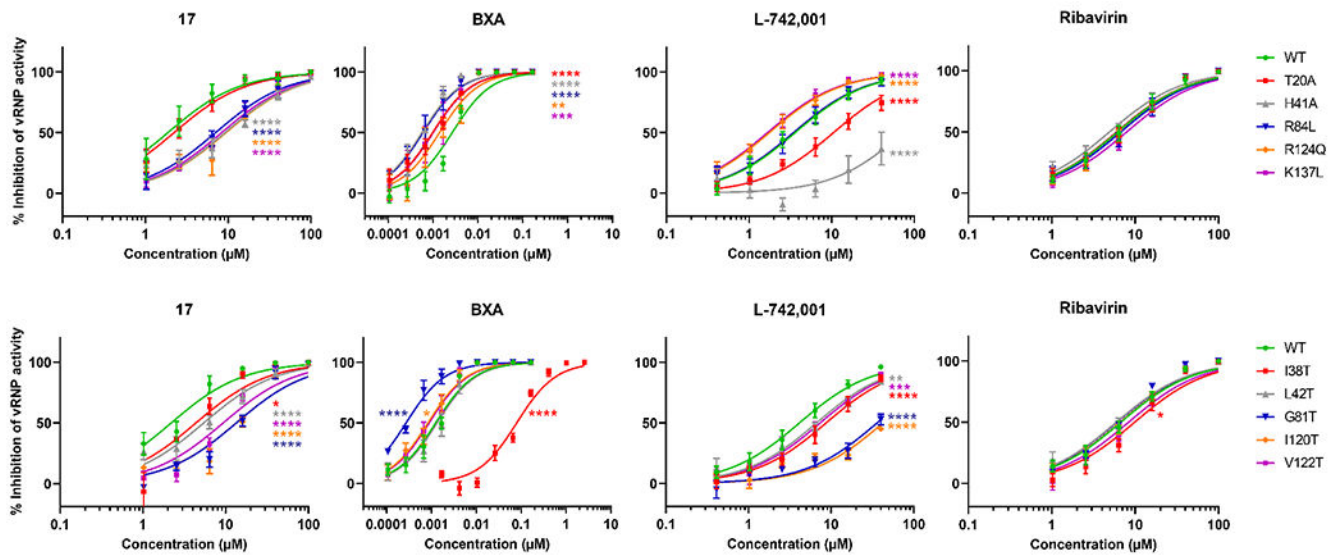


Figure 4.

Impact of mutations in or around the PA_N active site, on inhibitory effect in the minigenome assay. The dose-response curves of the different mutants were compared to wild-type with an extra-sum-of-squares F test (GraphPad Software, San Diego, CA, USA). P -values * 0.05; ** 0.01; *** 0.001; **** 0.0001.

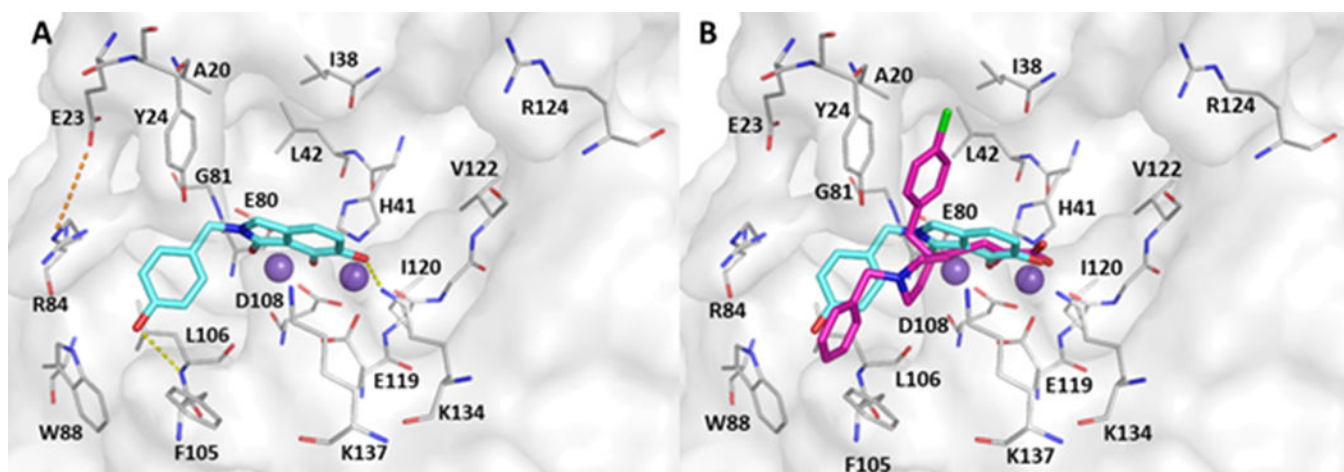
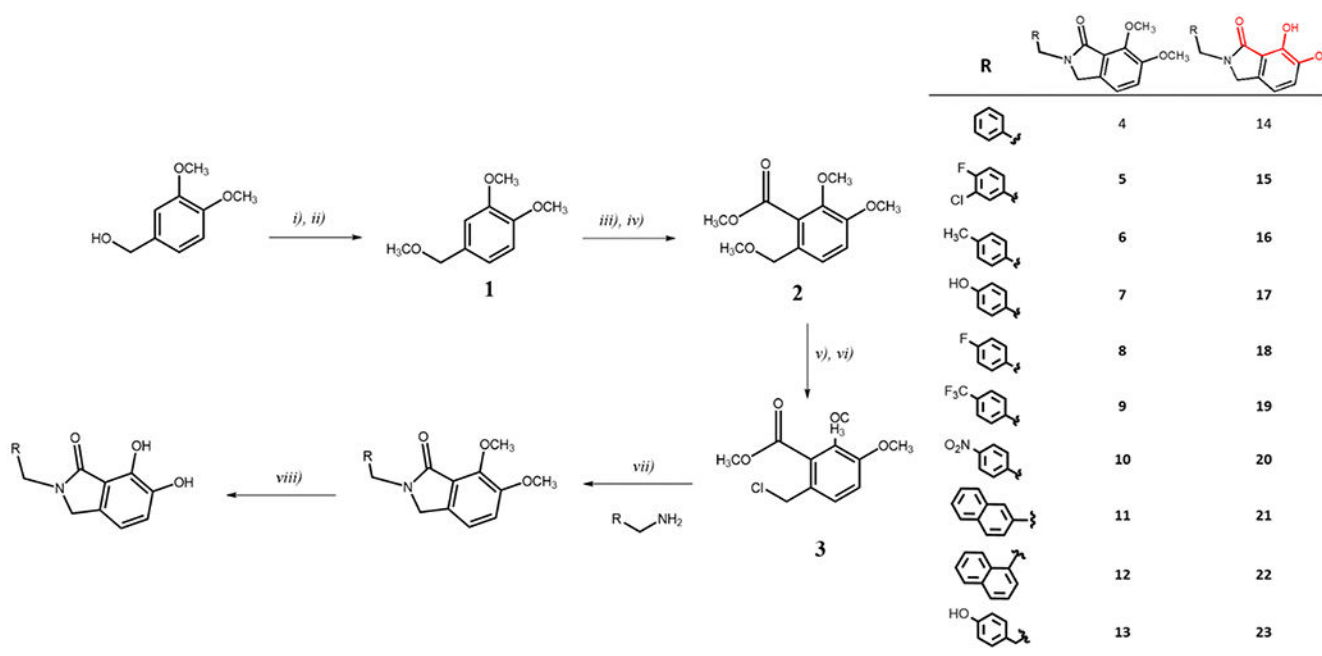


Figure 5.

A) Predicted binding mode for **17** (in cyan), based on compound docking in PA_N (from PDB code 4AWM). The two metal ions in the catalytic site are shown as purple spheres. Hydrogen bonds are shown as yellow dashed lines, while the electrostatic interaction between Arg84 and Glu23 is highlighted as an orange dashed line. B) X-ray pose of L-742,001 (in magenta; PDB 4E5H), superimposed on the predicted binding pose of **17** (in cyan).

**Scheme 1.**

Synthetic pathway to obtain the isoindol-1-ones **14-23**. Reagents and conditions: *i*) N_2 , THF, 0 °C, NaH, 30 min.; *ii*) CH_3I , then r.t., 3 hrs; *iii*) N_2 , 0 °C, Et_2O , *n*-BuLi, 3 hrs; *iv*) -80 °C, methylchloroformate, then r.t., 20 hrs; *v*) 0 °C, Et_2O , $ZnCl_2$; *vi*) acetylchloride, 30 min.; *vii*) CH_3CN , NEt_3 , reflux; *viii*) N_2 , -80 °C, CH_2Cl_2 , BBr_3 , then r.t., 4 hrs. The MBP is highlighted in red.

Table 1.

IC₅₀ values for compounds **14-23**, determined by FRET-based PA_N endonuclease assay. 2,4-dioxo-4-phenylbutanoic acid (DPBA) was used as a positive control.

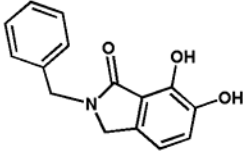
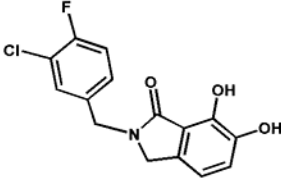
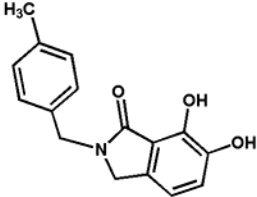
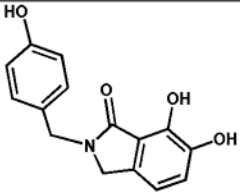
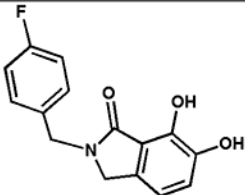
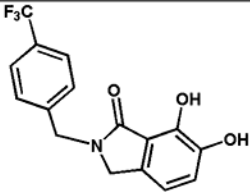
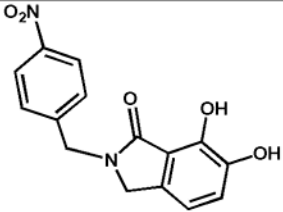
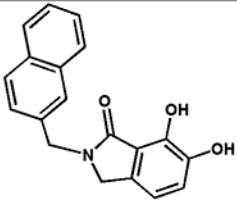
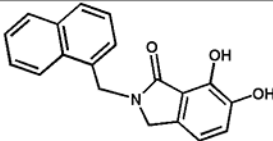
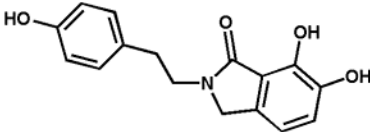
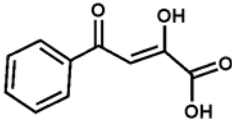
Structure and code IC ₅₀ (nM)	Structure and code IC ₅₀ (nM)	Structure and code IC ₅₀ (nM)
 14 46.7 ± 25.4 nM	 15 24.6 ± 7.2 nM	 16 30.6 ± 20.7 nM
 17 27.3 ± 7.5 nM	 18 23.6 ± 7.2 nM	 19 193 ± 55 nM
 20 36.6 ± 9.7 nM	 21 29.5 ± 15.1 nM	 22 128 ± 49 nM
 23 26.6 ± 5.7 nM	 DPBA 102.1 ± 32.2 nM	

Table 2.

Inhibition of influenza virus polymerase activity in the minigenome assay in HEK293T cells.

Compound	Inhibition of polymerase activity EC ₅₀ (μM) ^a	Cytotoxicity CC ₅₀ (μM) ^a
14	12	>100
15	3.6	>100
16	4.1	>100
17	4.2	>100
18	8.2	>100
19	19	>100
20	28	>100
21	5.4	>100
22	26	>100
23	19	53
BXA	0.0016	>2.6
L-742,001	5.0	>40
Ribavirin	11	>100

^aEC₅₀: compound concentration giving 50% reduction in the influenza vRNP-driven luciferase signal. CC₅₀: 50% cytotoxic concentration, estimated by ATP lite viability assay. Data from three independent tests were compiled to draw semi-log dose-response curves and calculate the EC₅₀ and CC₅₀ values by GraphPad Prism. BXA: baloxavir acid.

Table 3.

Inhibitory effect of compound **17** on PA-mutant forms of influenza virus polymerase, determined by minigenome assay in HEK293T cells.

PA form	17	BXA	L-742,001	Ribavirin
Fold increase in EC ₅₀ compared to wild-type				
WT	1.0	1.0	1.0	1.0
T20A	1.2	0.3	2.9	1.0
I38T	2.0	65	2.1	1.5
H41A	4.9	0.2	>11	0.8
L42T	2.5	1.1	1.6	0.9
G81T	6.1	0.2	8.7	0.9
R84L	3.8	0.2	1.0	1.1
I120T	6.1	0.7	>9.6	1.0
V122T	4.2	0.7	1.8	1.2
R124Q	5.0	0.5	0.5	1.1
K137L	4.5	0.4	0.5	1.3

Values shown represent the fold increase in EC₅₀ value for PA-mutant versus wild-type polymerase (EC₅₀: compound concentration giving 50% reduction in the influenza vRNP-driven luciferase signal). Data from three independent tests were compiled to draw semi-log dose-response curves and calculate the EC₅₀ values by GraphPad Prism. BXA: baloxavir acid.